In: Advances in Mechanics Research, Volume 1
Editor: Jeremy M. Campbell

ISBN: 978-1-61728-105-1

Chapter 5

COMPUTATIONAL FLUID DYNAMICS MODELING IN YARN ENGINEERING

Asis Patanaik[a*] and Rajesh D. Anandjiwala[a, b]

[a]CSIR Materials Science and Manufacturing, Polymers and Composites Competence Area, Nonwovens and Composites Group, P.O. Box 1124, Port Elizabeth 6000, South Africa

[b]Department of Textile Science, Faculty of Science, Nelson Mandela Metropolitan University, P.O. Box 77000, Port Elizabeth 6031, South Africa

ABSTRACT

This chapter deals with the application of computational fluid dynamics (CFD) modeling in reducing yarn hairiness during the ring spinning process and thereby "engineering" yarn with desired properties. Hairiness significantly affects the appearance of yarns and fabrics. The presence of a large number of hairs on yarn surfaces gives a fuzzy appearance to the resultant fabric and a greater tendency for pill formation in the fabric. As increasingly strict requirements are placed on yarns in high performance oriented weaving and knitting, the hairiness of yarns needs to be reduced to avoid entanglement of yarns and end breakages in subsequent processing. This has resulted in the development of new nozzle profiles to address the problem. The airflow pattern in the nozzles plays a significant role in the reduction of hairiness. CFD has been effectively utilized in yarn engineering to understand the actual mechanism of reducing yarn hairiness. The influence of different nozzle parameters such as diameter and axial angle of the nozzle in reducing yarn hairiness are investigated with the help of CFD. Other factors such as air pressure in the nozzles in affecting the tendency of reducing hairiness in different types of yarn are also investigated. The influence of drag force and impact angle of airflow on reducing yarn hairiness is also discussed. The yarns spun with the nozzles show a significant reduction in hairiness (36-60%) in comparison to the normal yarns spun without using nozzles. CFD modeling of airflow inside the nozzles provides a new direction in addressing the problem of hairiness characteristics in yarn engineering.

* Corresponding author: E-mails: patnaik_asis@yahoo.com; APatnaik@csir.co.za

INTRODUCTION

Yarns spun from staple fibers have protruding ends and loops of fibers projecting out of the yarn surface. These are commonly termed as 'hairs'. The amount of hairs quantified either in numbers or in total length per unit length of a yarn, is termed as hairiness. Yarn hairiness affects the appearance of staple yarns and the resulting fabrics as well as the efficiency of intermediate processes involved in converting the staple yarns into fabrics. Hairiness also affects apparel characteristics such as handle and thermal insulation. In the majority of cases yarn hairiness is undesirable like in formal wears, but in some cases it is desirable for example in case of some winter garments or fashion clothes [1].

Excessive hairiness on yarns affects the efficiency of knitting. Hairiness is of great disadvantage for warp yarns because it induces clinging tendency between them and thus causes warp breaks. Excessive hairiness causes fly generation during spinning and post spinning operations and this can be a health hazard to workers. Hairiness can cause frequent machine breakdowns and production of poor quality yarns. Yarn hairiness is one of the most serious causes of inefficiency in sizing, weaving, and knitting [1]. A very high level of yarn hairiness gives a fuzzy appearance to fabrics and the fabrics are prone to pill formation. It often causes uneven dyeing and color effects on fabrics.

Yarn hairiness depends on factors, such as fiber parameters, yarn structure and processing variables during yarn forming processes [1-11]. Among these processes, spinning plays a vital role in the formation of yarn hairiness. Yarn hairiness increases in winding and causing end breaks during warping and sizing. Because of the disadvantages associated with the yarn hairiness, many methods were developed to reduce it. Traditional methods of reducing yarn hairiness are: sizing in the short staple spinning and two-folding in the long staple spinning. Higher costs due to additional machine elements and time consumption are the major disadvantages associated with these methods. In recent years, several technologies have been developed to reduce yarn hairiness during spinning of which few have been commercialized. Compacting the fiber strand during drafting at the ring frame (Compact Spinning) [12-19] and placing an air-nozzle below the spinning triangle on the ring frame (jetring or nozzle-ring spinning) [20-31], are two recently developed techniques to reduce yarn hairiness. The main disadvantages of compact spinning is the cost of the spinning machine, chocking of the compacting elements (i.e. perforated drums, aprons) by fibers, and faster wear-out of top roller cots and aprons [1, 12].

Use of air-nozzles during ring spinning is referred to as 'nozzle-ring spinning', and this may offer cheaper alternative to compact spinning in reducing yarn hairiness. Nozzle-ring spinning combines the essential features of both ring and air-jet spinning technologies. The single nozzle, placed below the yarn formation zone, acts in a way similar to the first nozzle in air-jet spinning [1, 20-26].

The airflow pattern in the nozzles plays a significant role in the reduction of yarn hairiness. For better understanding the principles of reducing hairiness by nozzles, a simulation of airflow is essential to obtain velocity profiles, such as the axial, tangential and resultant velocities of air acting on yarn surfaces and hairs. Airflow simulation has been carried out by employing principles of Computational Fluid Dynamics (CFD). A comprehensive study was undertaken for the reduction of yarn hairiness in nozzle-ring spinning [20-26]. Positioning of the nozzle with respect to front roller nip (distance),

directions of airflow (linear and rotational), influence of air pressure, nozzle parameters viz. axial angle of air inlets and yarn channel diameter on reduction in yarn hairiness were investigated. A mechanism of reduction in yarn hairiness was proposed. Optimization of nozzle parameters, fiber linear density and air pressure on reduction in yarn hairiness has been carried out for polyester yarns spun from fibers of different linear densities. Quantification of drag forces acting on hair and yarn surface are of importance in describing the behavior of different nozzles on reduction in yarn hairiness. Drag forces acting on yarn and hairs were also computed. The angle of impinging of drag forces on hair was calculated and its role was also discussed [23].

Nozzles Fabrication and Mounting on the Ring Frame

Different set of nozzles were fabricated by varying the nozzle parameters, axial angle of air inlets and yarn channel diameters. All experiments were carried out by placing one nozzle (along with housing) at a time on one spindle of the ring frame [1, 20-26]. To place the nozzles at appropriate positions during ring spinning, nozzle-housings were fabricated and the nozzles were mounted inside the nozzle-housings [1, 21]. A typical angular view of the nozzle along with housing is shown in Figure 1 [24]. A schematic representation of the nozzle geometry has been described elsewhere [32]. The nozzle geometry is a combination of cylindrical and divergent sections. To create a swirling effect inside the nozzle, four air holes of 0.4 mm diameter were made tangential to the inner walls of the nozzles. A frame to mount the nozzle housing was fabricated after studying the geometry of the ring frame for exact positioning of the nozzle without altering the yarn path. A small ceramic guide was fixed at the bottom of the frame to keep the yarn at the centre of the nozzle. The nozzle was placed in such a way that the front roller nip and axes of nozzle, yarn, lappet and ceramic guide lay in a straight line. Compressed air was supplied to the nozzles through pipes with a pressure regulator and an air filter [1, 21].

COMPUTATIONAL FLUID DYNAMICS

Simulation of airflow inside the nozzle was carried out by CFD. Using the results of air velocity based on simulation, air drag forces and their directions were calculated.

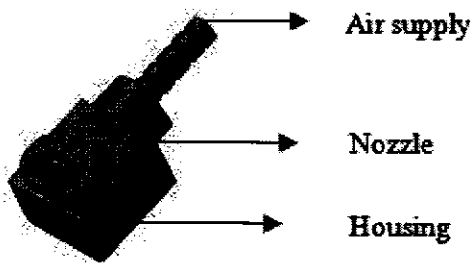

Figure 1. Angular view of the nozzle along with housing [Source: reference 24]

Airflow Simulation

To analyze the airflow pattern, simulation of airflow was carried out using a fluid flow analysis package, Fluent 6.1 [20-26, 33, 34]. To solve the three-dimensional airflow field inside the nozzles, a CFD model was developed using the above software. Fluid flow and related phenomena can be described by partial differentiation equations, which cannot be solved analytically except in over-simplified cases. To obtain an approximate solution numerically, a discretization method to approximate the differential equations by a system of algebraic equations, which can be then numerically solved on a computer. The approximations were applied to small domains in space and/or time so the numerical solution provides results at discrete locations in space and time. Much of the accuracy depends on the quality of the methodology used, for which CFD is a powerful tool to predict the flow behavior of fluid inside any object. It provides various parameters such as air velocity profiles (axial, tangential, resultant etc.) and path lines trajectory, which are important for subsequent analysis. It was for those reasons that a CFD package, Fluent 6.1, which uses a Finite Volume (FV) method, was employed for airflow simulation.

The Finite Volume (FV) method is the simplest method to understand and to program. The Finite Volume (FV) method uses the integral form of the conservation equations as its starting point. The solution domain was subdivided into a finite number of continuous control volumes (CVs), and the conservation equations were applied to each CV. At the centroid of each CV lies a computational node at which the variables are to be calculated. Interpolation was used to express variable values at the CV surface in terms of nodal (CV-centre) values. Surface and volume integrals were approximated using suitable quadratic formulae. By solving algebraic equations results for each CV were obtained, in which a number of neighbor nodal values appeared.

The simplest complete models of turbulence are two-equation models in which the solution of two separate transport equations allows the turbulent velocity and length scales to be independently determined. The standard k-ε model in Fluent falls within this class of turbulence model and has become the workhorse of practical engineering flow calculations. It is widely used for a range of turbulent flows in industrial flow and heat transfer simulations. It is a semi-empirical model and the derivation of the model equations which relies on phenomenological considerations and empiricism.

The Fluent package includes the following series of operations during the airflow calculations [33, 34]:

- Filters (translators) for import of surface and volume meshes from CAD/CAE packages such as Ansys, Cgns, I-Deas and others.
- Gambit, the preprocessor for geometry modeling and mesh generation.
- TGrid, an additional preprocessor that can generate volume meshes from existing boundary meshes (prePDF, the preprocessor for modeling non-premixed combustion in Fluent).
- Fluent, the solver.

The airflow in the developed nozzles was turbulent and hence the standard k-ε model of turbulence along with standard wall functions was used [1, 20-26]. The density weighted

average equation and continuity equations along with energy equation, turbulent kinetic energy equation and ε equation were solved in segregated solver [33, 34]. It has been assumed that the flow inside the nozzle affects the yarn but the presence of yarn inside the nozzle has no effect on airflow and hence yarn was not modeled during simulation [20-26]. The cross-sectional area occupied by the yarn inside the nozzle was very small compared to that of yarn channel of the nozzle (1:100). There are issues related to meshing of the zone near the yarn surface, hence it was not directly modeled in the simulation. High pressure and velocities of the air, coupled with considerably low volume of the yarn compared to that of yarn channel of the nozzle also justifies this assumption. A three-dimensional simulation model was used, because of the positioning of air inlets, air velocity is resolved into three components viz., axial (x-direction), tangential or swirling (y-direction) and inward radial velocities (z-direction) as shown in Figure 2. A very negligible amount of radial velocity was found because of the fluctuations in Z-axis was very small as compared to fluctuations in X- and Y-axes. When facing the nozzle outlet, anticlockwise rotation was taken as positive and clockwise rotation as negative in the simulation studies [1, 20-26].

In the present configuration, air inlet boundaries are assumed to be "*Pressure Inlet*" while outflow boundaries are assumed "*Pressure Outlet*". Pressure inlet boundary conditions were used to define the total pressure and other scalar quantities at flow inlets. Pressure outlet boundary conditions were used to define the static pressure at flow outlets. At the nozzle inlet, the air pressure was varied. At the nozzle outlet, the pressure was supposed to be the external pressure (one atmosphere). At the wall of the nozzle standard wall function boundary condition was applied. Although the high velocity of air stream was a heat source that will increase the temperature in the nozzle, the nozzle length was very short and the process occurs in a very short time. For simplification, it was assumed that the process is adiabatic i.e. no heat transfer occurred through walls. The flow model used was viscous, compressible airflow [1, 20-26].

The following series of equations were used to solve a compressible turbulent flow for airflow simulation [20-26, 33, 34];

Mass conversion equation:

$$\frac{\partial \rho}{\partial t} + \frac{\partial \rho u_i}{\partial x_i} = 0$$

Momentum conversion equation:

$$\frac{\partial}{\partial x_i}\left(\rho u_i u_j\right) = -\frac{\partial p}{\partial x_i} + \frac{\partial}{\partial x_j}\left[\mu\left(\frac{\partial u_i}{\partial x_j} + \frac{\partial u_j}{\partial x_i} - \frac{2}{3}\delta_{ij}\frac{\partial u_l}{\partial x_l}\right)\right] + \frac{\partial}{\partial x_j}\left(-\rho\overline{u'_i u'_j}\right)$$

Turbulent kinetic equation:

$$\frac{\partial\left(\rho k u_i\right)}{\partial x_i} = \frac{\partial}{\partial x_j}\left[\left(\mu + \frac{\mu_t}{\sigma_k}\right)\frac{\partial k}{\partial x_j}\right] + G - \rho\varepsilon$$

Rate of dissipation of the turbulent kinetic energy:

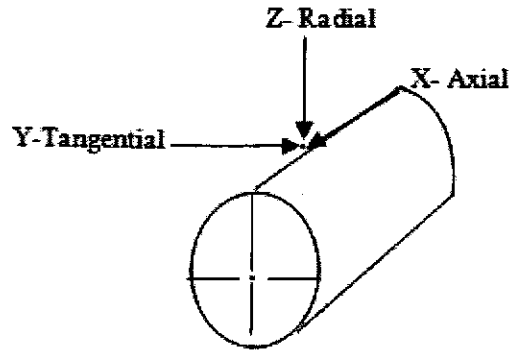

Figure 2. Representation of air velocity components [Source: reference 23]

$$\frac{\partial (\rho \varepsilon u_i)}{\partial x_i} = \frac{\partial}{\partial x_j}\left[\left(\mu + \frac{\mu_t}{\sigma_\varepsilon}\right)\frac{\partial \varepsilon}{\partial x_j}\right] + c_1 \frac{\varepsilon}{k} G - c_2 \rho \frac{\varepsilon^2}{k}$$

The Nomenclature used is given below:

ρ = density of air, t = time, u = velocity of air, p = static pressure, u_i = fluctuation in u in x-direction, $\overline{\rho u'_i u'_j}$ = Reynolds stress tensor, δ_{ij} = Kronecker's delta function, G = rate of generation of turbulent kinetic energy, k = turbulent kinetic energy, μ_t = turbulent viscosity, ε = rate of dissipation of turbulent kinetic energy and $c_1, c_2, \sigma_k, \sigma_\varepsilon$ constants of the k-ε model.

The structure of airflow inside the nozzle depends on the following factors: angle at which air enters into the nozzle (or axial angle of air inlets), channel diameter (or yarn channel diameter) and air pressure. The configurations studied were as follows: axial angle of air inlets; 40°, 45°, 50°, yarn channel diameter; 1.8, 2.2, 2.6 mm and air pressure; 0.5, 0.7, 0.9. The length of the yarn channel was 17 mm. The diameter of air entry orifice was 0.4 mm. From the simulation, airflow pattern, components of air velocity (axial, tangential and resultant) at different normal planes for various nozzles were obtained.

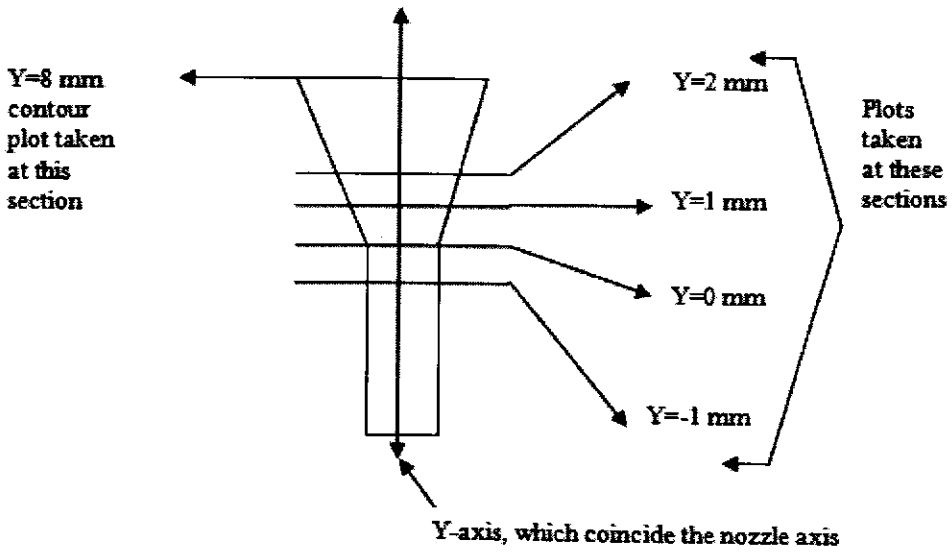

Figure 3. Notations of normal planes [Source: reference 23]

To get air velocity profiles on different normal planes of nozzles, various sections of the nozzle were considered at a distance of 1 mm, along the axis of the nozzle (Figure 3). The throat of nozzle was considered as origin (x = 0 and y = 0). Figure 4 shows the axial, tangential and resultant air velocity plots for the nozzle having axial angle of air inlets 40° and yarn channel diameter 1.8 mm at a pressure of 0.5 bar. Each color represents a particular air velocity values in m/s. Similarly, air velocity contours were obtained for other nozzles which will be discussed in following sections.

Calculation of Air Velocity on Yarn Surfaces and Hairs

To calculate air velocity acting on the surfaces of yarn and hairs, a 30 tex nozzle-ring spun cotton yarn was considered. Using a microscope (Leica) and software yarn diameter was measured. The measured diameter of yarn was 0.246 mm. A solid cylinder of 0.246 mm (analogues to yarn) was superimposed on the air velocity profile obtained at various normal planes of the nozzle by using post processing software in such a way that the cylinder was coaxial to the nozzle axis. From this, air velocity acting on yarn surface can be computed. As mentioned previously in the simulation section, it was assumed that presence of yarn did not affect the airflow but the airflow affected the yarn. However, the presence of yarn inside the nozzle certainly alters the airflow, which cannot be determined with the model used in this study for airflow simulation [1].

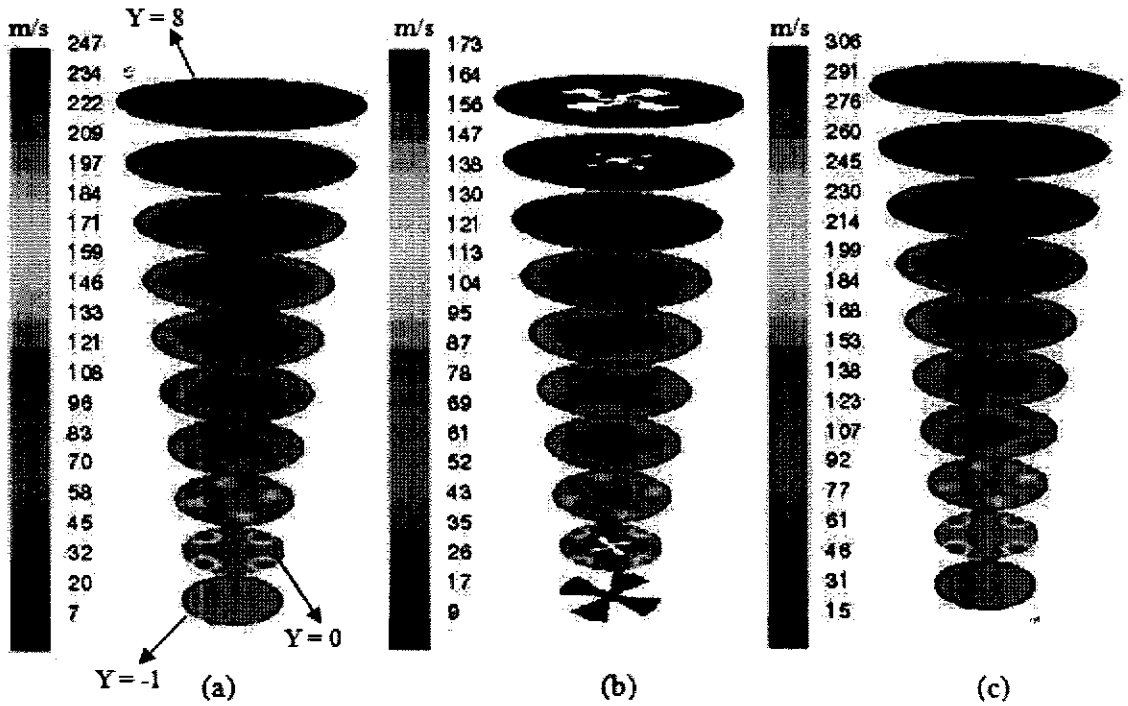

*White color shows velocity magnitude of -1 m/s for (b)

Figure 4.Air velocity plots for a nozzle: (a) axial; (b) tangential and (c) resultant velocity [Source: reference 23]

As seen from Figure 4, air velocity reduces from wall to axis of the nozzle. The cross-sectional area occupied by the yarn was very small compared to that of yarn channel of the nozzle (approximately 1:100). As a result air velocity acting on yarn surfaces, calculated using the post processing software for yarns of different diameters or linear density, are nearly the same [1]. The resultant air velocity acting on hairs was calculated by considering the particular length of hairs (mm) at various planes of the divergent section of the nozzle. Since hairs of numerous configurations and orientation are found on a spun yarn, calculations of air velocities on these would be an extremely time consuming job. Consequently, a simplified approach was adopted wherein, hair was assumed to lie perpendicular to the yarn [32]. Longer hairs may bend inside the nozzle while touching the wall of the nozzle due to the space constraint. Because of the reducing air velocity gradient from the wall of the nozzle to the yarn surface, a hair in the vicinity of the nozzle-wall was subjected to a maximum drag force, whereas the base of the hair (at yarn surface) would be subjected to a minimum air drag force (Figure 4). The maximum length of projecting hair on a yarn kept inside the nozzle varies along the nozzle due to the variation in inner diameter and the presence of divergent section.

Air Drag Forces Acting on Yarn Surface and Hair

When a yarn is subjected to airflow, the flow can be split into two mutually perpendicular directions: parallel and perpendicular to the yarn axis. The forces exerted on a body by the longitudinal (parallel to nozzle axis) and transverse (normal to nozzle axis) airflows are given by the respective longitudinal and transverse drag forces. In fluid dynamics, equations have been developed to quantify the drag forces on smooth circular cylinders which were analogous to yarns [35-37]. The longitudinal drag force (F_l) or (LDY) on yarn is given by:

$$F_l = \frac{1}{2} \rho V_l^2 S_l C_{Dl}$$

where, ρ = density of the air (kg/m^3);
V_l = the relative velocity between air (inside the nozzle) and yarn (m/s);
S_l = the surface area of the yarn on which the parallel airflow acts (m^2);
C_{Dl} = the air-drag coefficient for longitudinal airflow (a dimensionless number).

C_{Dl} is related to the Reynolds number as: $R_e = \dfrac{V_l d_y}{\mu / \rho}$

where, d_y = the diameter of the yarn (m);
μ = the viscosity of air (N s/m^2).

The surface area of a yarn (cylindrical body) is given by:

$$S_l = \pi d_y l$$

where, l is the length of the yarn (m).

Transverse drag force (F_t) or (TDY) on yarn is given by:

$$F_t = \frac{1}{2} \rho V_t^2 S_t C_{Dt}$$

where, ρ = density of the air (kg/m^3);

V_t = the relative velocity between air (inside the nozzle) and yarn (m/s);

S_t = the surface area of the yarn on which the transverse airflow acts (m^2);

C_{Dt} = the air-drag coefficient for transverse airflow (a dimensionless number).

C_{Dt} is related to the Reynolds number as: $R_e = \frac{V_t d_y}{\mu / \rho}$

where, d_y = the diameter of the yarn (m);

μ = the viscosity of air (N s/m^2).

The surface area of a yarn (cylindrical body) is given by:

$$S_t = d_y l$$

where, l is the length of the yarn (m).

Under standard testing conditions, ρ = 1.197 kg/m^3 and $\mu = 18.22 \times 10^{-6}$ N s/m^2 [35, 36]. Hence, for a given yarn diameter and relative speed between air and yarn, R_e can be calculated for the above equations. Once R_e is known, C_D can be obtained from the established relationship between the drag coefficient and Reynolds number for circular cylinders [35-38]. Similarly, longitudinal (LDH) and transverse drag forces (TDH) on hairs can be calculated by taking the respective velocities on hair surfaces.

APPLICATION OF CFD IN YARN ENGINEERING

This sections deals with the application of CFD in conjunction with experimental data in reducing yarn hairiness during ring spinning. Effects of airflow direction, nozzle distance from front roller nip and air pressure in reducing yarn hairiness were discussed along with the mechanism of reduction in yarn hairiness. The influence of different nozzle parameters in reducing hairiness in yarns of different linear densities and optimization of nozzle parameters, fiber linear density and air pressure were also studied. The influences of drag force and impact angle of airflow on tendency to reduce yarn hairiness were also discussed. Tensile and evenness properties of nozzle-ring spun yarns and yarns spun without nozzle (control) were compared. The pilling tendency of fabrics produced from the nozzle-ring yarns were compared with the fabrics that produced from the control yarns.

Effect of Airflow Direction on Hairiness Values of Nozzle-ring Spun Yarns

The influence of airflow direction on hairiness values of nozzle-ring spun yarns has been reported [1, 21]. Z-twisted 30 tex carded cotton yarns were spun with and without nozzles (i.e. nozzle-ring spun yarns and control yarns, respectively) on a ring frame. The spinning process parameters employed to produce both the nozzle-ring spun yarns and control yarns were as follows: spindle speed 16000 rpm; traveller type and number EM1 UDR 2/0; and twist per inch (tpi) 19.6. For nozzle-ring spinning, nozzle 50-2.2 (50° axial angle of air inlets and 2.2 mm yarn channel diameter) was placed between the front roller nip and lappet guide on the ring frame. The nozzle was placed in two configurations to have the resultant direction of airflow one in upward (i.e. towards front roller) and the other in downward (i.e. towards lappet). Air pressures of 0.5, 0.7 and 0.9 bar, distances of the nozzle from the front roller nip 4, 7 and 10 cm were selected for the study. Distances longer than 10 cm could not be employed as the top most position of lappet during cop building touched the nozzle holding frame. Similarly, distances shorter than 4 cm were not possible due to the difficulty in fixing the nozzle to the nozzle holding frame.

Yarn samples were kept in standard atmosphere (i.e. temperature 20±2°C, relative humidity, 65±2%) for 24 hours prior to testing. The hairiness of yarns was tested on Zweigle G 566 hairiness tester [1, 21]. The number of hairs protruding from the yarn, N1, N2, N3, N4, N6 and N8 (i.e. lengths of hair equal to or exceeding 1 mm, 2 mm, 3 mm, 4 mm, 6 mm and 8 mm, respectively) were obtained. S3 hairiness value is the sum of the values N3, N4, N6 and N8. For each sample, 800 meters of yarn was tested at a speed of 50 m/min. To compare the hairiness values of ring and nozzle-ring spun yarns and among different nozzle-ring spun yarns, S3 hairiness values of nozzle-ring spun yarns were normalized as:

$$\text{Normalized S3 hairiness values} = \frac{\textit{Number of hairs on the nozzle} - \textit{ring spun yarn}}{\textit{Number of hairs on the ring spun yarn}} \times 100$$

Yarn diameters and helix angle of surface fibers and wrapped hairs by the nozzle (discussed in subsequent section) were measured on a Leica MZ6 microscope using Leica software. The yarn diameters and helix angles were measured randomly at 1000 and 100 places, respectively [21].

Table 1 shows the hairiness values of ring spun (C) and nozzle-ring spun cotton yarns [1, 21]. S3 hairiness values of nozzle-ring spun yarns under upward airflow were lower by an order of 36-58% compared to that observed in the control yarn and this reduction in S3 hairiness values are statistically significant. Downward airflow was ineffective in reducing yarn hairiness (Table 1) and this may be due to the fact that the majority of the protruding fiber ends correspond to trailing ends [2, 7, 21]. It is logical to believe that the reduction in yarn hairiness may be more efficient when the air vortex induces an axial airflow in a direction opposite to that of yarn, meeting a majority of protruding fiber ends (i.e. trailing hairs) and pushing them within yarn body more easily than the leading ends [21, 30]. The downward airflow may raise the trailing fiber ends and, therefore, the airflow along the direction of yarn movement may promote, rather than suppress the protruding fiber ends [21, 28]. It was observed (Table 1) that, with the downward airflow, the number of hairs was very large in all hair-length groups when compared to the control sample [1, 21]. The S3 hairiness

values of nozzle-ring spun yarns under downward airflow were higher than that of control yarn by an order of 90-240%.

Mechanism of Hairiness Reduction in Nozzle-ring Spinning

The path lines of air released from the air inlets of a nozzle is shown in Figure 5 [1, 21, 25]. The resultant (or total) air velocity is resolved into three components viz. axial, tangential and radial, respectively. Swirling of airflow was created by the tangential and axial velocity components of air velocity. All four air holes in the nozzle lie on the same horizontal plane. Absence of staggering of air inlets helps to generate swirling airflow, as air coming from one air inlet does not intrude with the other; rather, airflow coming from all four air inlets spirals around the yarn resulting in this type of flow. Contours of resultant velocity of air are shown in Figure 6, at ten normal planes along the axis of the nozzle [1, 21]. The air velocity profile along with velocity components for another nozzle (45-2.2) is shown in Figure 7 [20]. The swirling airflow action in the nozzle, irrespective of different nozzle types, remains same; only the magnitude varies as per the design parameters of the nozzle. Air velocities viz., Vty and Vay represents tangential and axial velocity acting on yarn surface and velocities viz., VTy and VTh (near inner wall of the nozzle) represents resultant air velocity acting on yarn surface and hairs, respectively (Figure 7). The radial velocity component is not shown in Figure 7 as it is very small in comparison to the other two components. It was observed that air was coming through the cylindrical portion of the nozzle at constant velocity, while near the neck, air velocity increased suddenly (Figure 7). This sudden increase in air velocity was due to the presence of the four air inlets at the neck of the nozzle, the air stream from them mixes with the air coming through the cylindrical portion of the nozzle creating a swirling effect. After that, air velocity decreases due to the presence of divergent portion of the nozzle, where air diffuses very quickly. The trends of resultant velocity acting on the yarn surface and hairs were similar except that hairs were subjected to a higher air velocity due to a reducing air velocity gradient from nozzle inner wall to axis of the nozzle. Axial air velocity follows the trend of resultant air velocity. The tangential air velocity at the centre of nozzle was almost constant in the divergent portion from 0.002 m to 0.008 m normal planes of the nozzle [1, 20].

The yarn passes through the centre of the nozzle; whereas the protruding fibers/hairs lie near the inner wall of the nozzle [1, 21]. Average resultant air velocity at the centre of the nozzle is 2220 m/min (37 m/s), as seen from Figure 6, and this was much higher than yarn speed (in the order 20 m/min at spindle speed of 16000 rpm). It was observed that the airflow was swirling in anticlockwise direction when the nozzle was viewed from top in the case of upward airflow. Due to the action of this air vortex or swirling air, the yarn body was untwisted when it entered the nozzle [21]. Other legends in Figure 7 represent various velocity parameters. In the region from 0 to 0.008 m axial distance, untwisting of Z-twisted yarn in S-direction and folding and wrapping of hairs around the yarn body in S-direction take place. Between the regions from 0 to 0.003 m, most of the untwisting of yarn and wrapping of protruding fibers is likely to take place as the resultant air velocity found in these regions was very high compared to that observed in the regions from 0.004-0.008 m. The air swirls at higher intensity in the former regions than in the later regions. Re-twisting of yarn

takes place in the regions from 0 to -0.008 m due to false twist effect on the yarn and the fact that airflow in these regions were not swirling (refer Figure 5). Consequently, the yarn gets back its original twist (Z) if there was no hysteresis during untwisting and twisting process of the yarn [20].

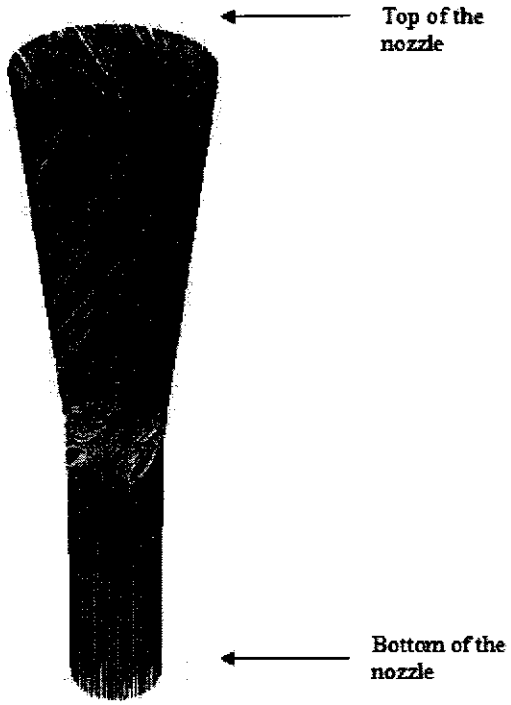

Figure 5. Typical path lines of air inside the nozzle [Source: reference 25]

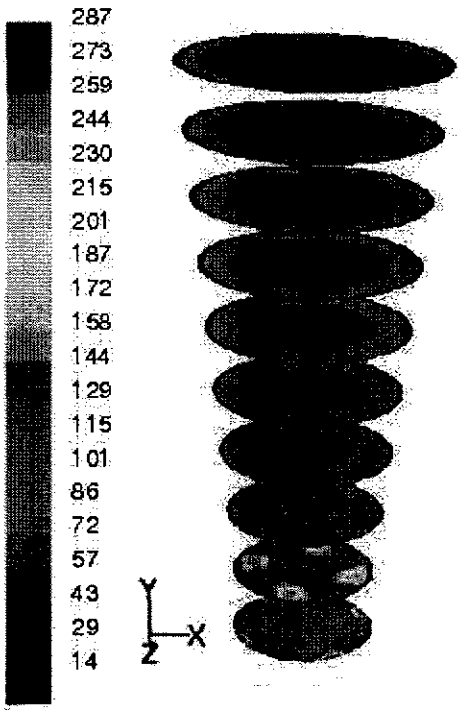

Figure 6. Contours of total (resultant) velocity air (m/s) [Source: reference 21]

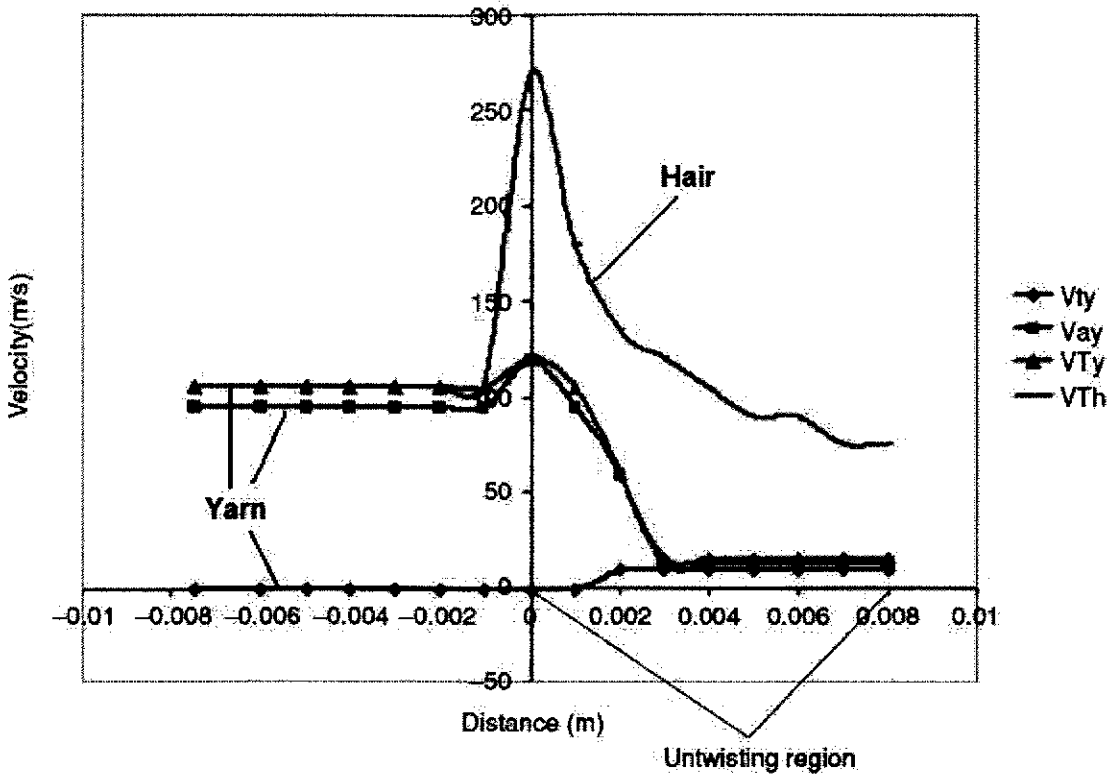

Figure 7. Air velocities acting on yarn and hair inside nozzle (45°, 2.2 mm) [Source: reference 20]

To observe how protruding fibers (trailing hair) wrap around the yarn when a yarn enters the nozzle and configuration of such fibers after the yarn leaves the nozzle by the action of air vortex; some artificial trailing hairs were prepared on a Z-twisted cotton yarn with a twist per inch of 19.6 [1, 21]. Red colored fibers were glued randomly with one of their ends on the surface of this yarn leaving the other end free. The prepared cotton yarn was passed through the nozzle placed in between the front roller nip and lappet. Air was then supplied to the nozzle. Yarn sections above and below the nozzle (i.e. after passing through the nozzle) were fastened to paper windows. This work was repeated several times at random intervals. Red colored fibers in Figure 8a and 8b show the direction of wrapped hairs on yarn at the top (nozzle entry) and bottom (nozzle exit) of the nozzle, respectively. It can be seen from Figure 8a, that when the yarn was at the entry side of the nozzle, a hair (colored fiber) was wrapped on yarn surface in S-direction and the Z-twisted yarn was untwisted such that it exhibited S-twist. Similarly from Figure 8b, it can be seen that as the yarn leaves the nozzle, the wrapped hairs and yarn twist were in Z-direction, due to false twisting effect of the yarn. Average helix angle of wrapped colored hairs and helix angle of surface fibers were 37° and 25°, respectively on the yarn above the nozzle [1, 21]. The mass of a hair is very negligible compared to that of yarn. Further, the hair was subjected to air moving at higher velocity than the yarn. Due to these reasons hair was rotated over the yarn (wrapped) at higher speed than the yarn, and conforms to a higher helix angle than the surface fibers [1, 21]. Average helix angles of wrapped colored hairs and surface fibers were 29° and 28°, respectively on the yarn at bottom of the nozzle. Measured diameters of yarn segment above and below the nozzle were similar (0.0246 cm) [1, 21].

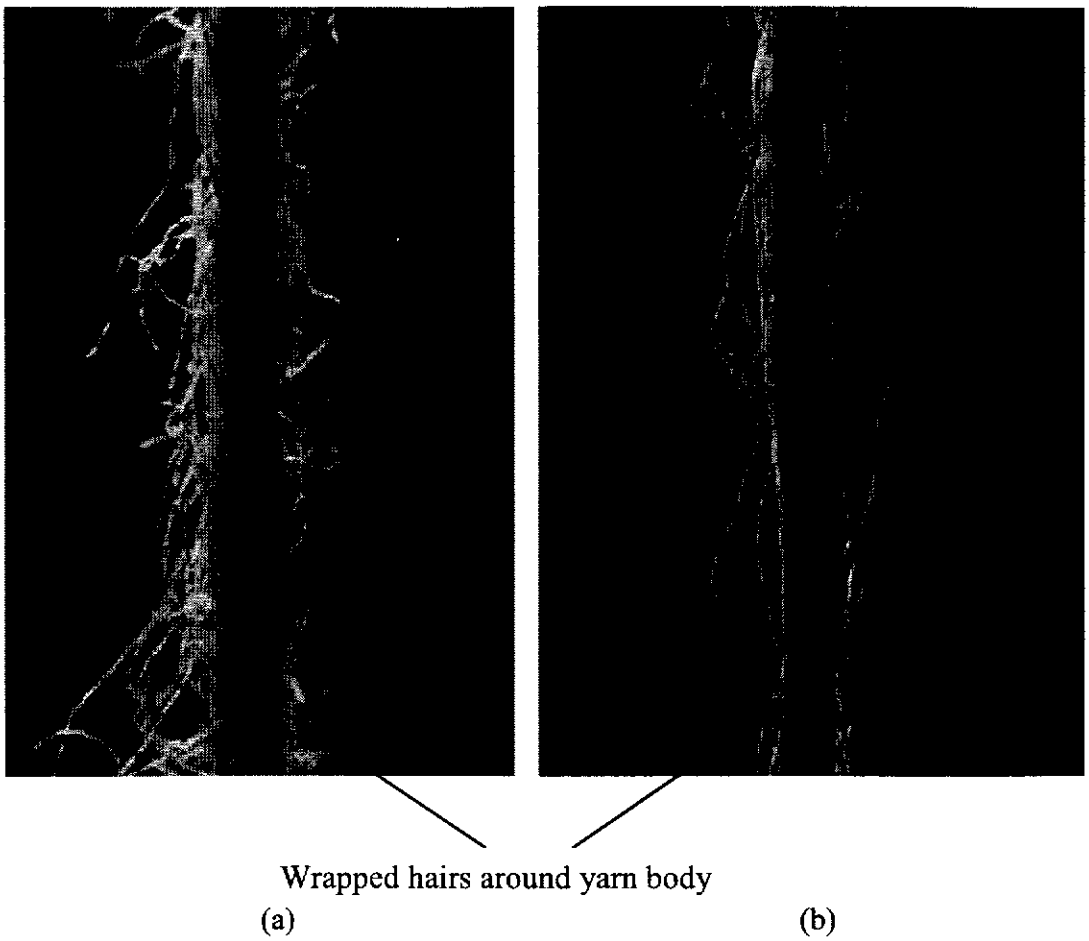

Figure 8. Photographs of nozzle-ring spun yarns with upward airflow at (a) top of the nozzle (b) bottom of the nozzle [Source: reference 21]

Yarn twists of 15.3 inch^{-1} and 17.4 inch^{-1} were observed for yarn sections at entry and exit of the nozzle, respectively [1, 21]. Yarn at the top of the nozzle was twisted to an extent 34.9 inch^{-1} (19.6 + 15.3). Due to false twisting action, the yarn was re-twisted to an extent 32.7 inch^{-1} (15.3 + 17.4). Due to hysteresis, final twist remaining in the yarn (i.e. 17.4 inch^{-1}) was lower than the original twist, 19.6 inch^{-1}, nevertheless, the final twist in the yarn was close to the original twist [1, 21].

Basically, hairs are produced in the yarns because the edge fibers (hairs) escape the twisting action. Yarns produced without nozzle (control sample) was twisted in the Z-direction. In control sample the hairs have no direction of twist. In nozzle-ring spinning, the edge fibers which are protruding out of the main fibrous strands initially get wrapped around the yarn body by the swirling air in S-direction at the top of the nozzle. As soon as the yarn passes through the nozzle the wrapped edge fibers are twisted in the opposite direction by the false twisting action to a twist level similar to that observed for the surface fibers [1, 21]. A hypothesis for the mechanism of hairiness reduction by nozzle under upward airflow has been proposed as follows [1, 21]: It was observed that suction air (from atmosphere) was rushing inside the nozzle without swirling from the bottom of the nozzle (Figure 5). Re-twisting of the yarn due to false twisting action can only take place at the bottom part of the nozzle i.e. when the yarn leaves the normal plane containing the air inlets. The resultant velocity of this straight air current was around 80 m/sec (Figure 6). It may be possible that with this high

velocity of air current, the resulting air drag acting normal to the spirals of the wrapped hair presses and spaces them out during retwisting of the yarn. This increases the pitch of these spirals in the S-direction. The pressure acting on the wrapped spirals enhances the friction between wrapped hair and the yarn surface which has spiral rugosities due to helical configuration of surface fibers, and consequently the wrapped fibers were aligned tightly along with surface fibers and the combined entity undergoes re-twisting. In the process, the helix angles of surface fibers and wrapped hairs would become nearly the same after the re-twisting process. The above experiment conducted on formed yarn with incorporation of artificial hairs differs from the actual process; nevertheless the mechanism of wrapping of hairs, yarn untwisting and retwisting and sequence of events would fundamentally remain the same for both the cases. In any event, the wrapping of hairs around yarn body by swirling air serves the purpose of reducing yarn hairiness [1, 21].

Effect of Distance of Nozzle from Front Roller Nip on Hairiness Values of Nozzle-ring Spun Yarns

The influence of distance of the nozzle from front roller nip on hairiness is given in Table 1. Hairiness decreases with increasing distance of the nozzle from the front roller nip for all the levels of air pressure and for both the cases of upward and downward airflows [1, 21].

When the nozzle was placed very close to the nip of the front roller at 4 cm, two events can be considered which influence reduction or increase in yarn hairiness [1, 21]:

- With an upward airflow, (a) disturbance to the fiber strand at the spinning triangle was very large due to the intensity of air currents impinging on the fiber strand; (b) the swirling airflow was such that it untwisted the fiber strand against the real twisting imparted to the fiber strand by the traveller, the length of fiber strand being small, the untwisting effect was quite large which hindered the yarn formation process.
- With downward airflow, (a) disturbance to the fiber strand at the spinning triangle was also very large due to the intensity of suction air currents entering the nozzle at yarn entry side; (b) the swirling airflow was such that it twisted the fiber strand in addition to the real twisting imparted to the fiber strand by the traveller, the length of fiber strand being small, the twisting effect was quite large, the effect which is not known.

Since the hairiness was found to increase with decreasing distance of the nozzle from front roller nip, for both the cases of upward and downward airflows, it may be concluded that the disturbance caused by the airflow to the fiber strand was larger when the nozzle was placed closer to the front roller compared to that placed at a longer distance (10 cm), thereby affecting the yarn formation [1, 21]. Further, it may result in some fiber loss when placed closer to the front roller. With the increasing distance of the nozzle from the front roller nip, the intensity of the air currents causing disturbance to spinning triangle decreases, and this may be the reason for getting a comparatively lower S3 hairiness values on yarn when the nozzle was placed at a longer distance than when it was placed at a shorter distance [1, 21].

Effect of Air Pressure on Hairiness Values of Nozzle-Ring Spun Yarns

When air pressure was increased from 0.5 to 0.9 bar a greater reduction in S3 hairiness values were observed as shown in Table 1 [1, 21]. With the increase in air pressure, the resultant air velocity increases, thereby increasing the transverse drag forces acting on the protruding hairs, making it easier for them to fold the hairs. Both the axial and tangential air velocity components also increase with the increase in air pressure, thus increasing the swirling intensity, consequently improving the wrapping of fibers around yarn body and hence, more reduction in hairiness. An air pressure of 0.5 bar was sufficient to reduce the yarn hairiness to a significant extent, and it is also economical to operate the nozzle at lower air pressure [21].

Influence of Axial Angles of Air Inlets on S3 Hairiness Values of Nozzle-ring Spun Yarns

The response of different nozzle parameters on hairiness of 100% cotton yarns was studied by varying the yarn linear density [1, 22]. Z-twisted carded cotton yarns of 10, 20 and 30 tex were spun with and without nozzles at a spindle speed of 16000 rpm. To investigate the effect of axial angles of air inlets on yarn hairiness, three nozzles, all having the same yarn channel diameter 2.2 mm and different axial angles of air inlets of 40°, 45° and 50° were selected (axial angle of air inlet series). To investigate the effect of yarn channel diameters of nozzles, three nozzles with different channel diameters 1.8, 2.2 and 2.6 mm, but all having the same axial angles of air inlets of 40° were selected (yarn channel diameter series). Based on previous experiments [21] an air pressure of 0.5 bar was considered sufficient for reducing yarn hairiness and this air pressure level was selected to operate the nozzles. Similarly, the direction of airflow was selected as upward and the distance of the nozzle from the front roller nip was kept at 10 cm [21].

Hairiness values of nozzle-ring spun yarns and conventional spun cotton yarns are shown in Table 2 [22]. Nozzle-ring spun yarns have a lesser number of hairs than the corresponding ring spun cotton yarns. For the nozzle angle series of experiments (J1-J9 in Table 2), 45° axial angle of air inlets showed the largest reduction in S3 hairiness values followed by nozzles with 40° and 50° axial angles of air inlets, when the yarn channel diameter was kept constant at 2.2 mm [1, 22]. This trend is similar for all the yarns, viz., 10, 20 and 30 tex yarns. S3 hairiness values of nozzle-ring spun yarns are significantly lower compared to that of control yarns. Using the results of simulation, the best performing nozzle 45-2.2 and the least performing nozzle 50-2.2 are analyzed and discussed here after.

Resultant velocity of air acting on the surface of yarn and hair in the case of nozzle with 45° axial angles of air inlets was higher compared to that of the nozzle with 50° axial angle. So the swirling intensity created by the nozzle with 45° axial angles was stronger than that of the nozzle with 50° axial angle, resulting in the higher reduction in yarn hairiness by the former. This was identified as the major reason [1, 22]. Apart from this, negative axial air velocity inside the nozzle may also play a role in lowering the efficiency of reduction in yarn hairiness. This negative axial air velocity gives jerkiness or unsteady motion to the yarn resulting in eccentric placement of the yarn inside the nozzle and yarn ballooning which may

affect wrapping of hairs around yarn body, as wrapping of hairs is a prerequisite for reducing yarn hairiness. Some amount of negative axial air velocity was found for the nozzle with 50° axial angle of air inlets. Negative axial air velocity was absent for the nozzle with 45° axial angle of air inlets. Yarn spends a prolonged period in the jerkiness zone in the nozzle having 50° axial angle. Since the yarn and protruding hairs were subjected to jerkiness of air currents acting on them for a comparatively long duration, efficiency of reducing yarn hairiness was less for the nozzle with 50° axial angle of air inlets when compared to the nozzle with 45° axial angle, where negative axial air velocity was absent [20, 22]. The axial angle of air inlet plays a significant role in reducing the yarn hairiness [20, 22].

The transverse (TDH) and longitudinal (LDH) drag forces acting on hair/fiber (calculated diameter of 11.6 μm) with the nozzles having different axial angles of air inlets was studied [1]. The transverse drag forces acting on hair with 45° axial angle of air inlets was higher in comparison with the other axial angles of 40° and 50°, resulting in higher bending moment on hairs and greater reduction in yarn hairiness. There was not much difference in the values of drag forces with axial angles of 40° and 50°. The longitudinal drag force with 45° axial angle was higher in comparison to the others. Transverse drag forces are responsible for laying down hairs over the yarn, while wrapping of the hairs was also facilitated by the action of yarn rotation and friction between surface fibers of yarn and the hairs.

Influence of Yarn Channel Diameter on S3 Hairiness Values of Nozzle-ring Spun Yarns

In the yarn channel diameter series of experiment, the nozzle with yarn channel diameter of 2.2 mm gives the largest reduction in S3 hairiness values, very closely followed by the nozzle of 1.8 mm and lastly the nozzle with 2.6 mm diameter. This trend was observed for all the yarn counts Table 2 [22]. Using the results of CFD modeling, the role of yarn channel diameter was analyzed by comparing two extreme values of yarn channel diameters i.e. 2.2 mm and 2.6 mm (the best and least performing, respectively).

The difference between the S3 hairiness values of yarns spun using nozzles with 2.2 and 2.6 mm diameters were statistically significant [1, 22]. Higher air velocity was observed inside the nozzle of 2.2 mm diameter, whereas it was much lower in the case of the nozzle with 2.6 mm yarn channel diameter. The swirling intensity created by the nozzle of 2.2 mm yarn channel diameter was stronger than that of the nozzle with 2.6 mm yarn channel diameter, thereby resulting in a greater reduction in yarn hairiness by the former. Negative axial velocity was observed for nozzle of 2.2 mm yarn channel diameter, which was absent for the nozzle of 2.6 mm yarn channel diameter.

For both the nozzles, the magnitude of tangential air velocity acting on the yarn body was different [1, 22]. A nozzle having yarn channel diameter of 2.2 mm gives slightly higher tangential air velocity (average value of tangential velocity from y = -1 to y = 8 planes was 8 m/s) when compared to that having a yarn channel diameter of 2.6 mm (5 m/s), as shown in Figure 9 [22]. Tangential air velocity contour plots were taken from y = -1 to y = 8 planes. A higher tangential air velocity gives rise to a faster swirling of air in the former as compared to the later, leading to efficient wrapping of hairs. For both the nozzles, some amount of

Table 1. Hairiness values of ring and nozzle-ring spun cotton yarns in upward and downward airflow [Source: Reference 21]

Code	*Nozzle distance (cm)	Air pressure (bar)	Number of hairs/100 m length of yarn														Normalized	
			N1		N2		N3		N4		N6		N8		S3		S3 hairiness values	
C			2880		283		83		39		8		1		131		100	
			(5.52)		(6.22)										(3.23)			
			U	D	U	D	U	D	U	D	U	D	U	D	U	D	U	D
S1	4	0.5	2569	4952	220	722	58	267	20	143	6	42	0	2	84	454	64	346
			(5. 23)	(5.14)	(6.15)	(6.23)									(3.11)	(3.27)		
S2	7	0.5	2350	3833	193	465	51	178	16	94	5	43	0	2	72	317	55	242
			(5.13)	(5.25)	(6.29)	(6.43)									(3.29)	(3.17)		
S3	10	0.5	2273	3433	187	396	44	153	16	94	5	29	0	1	65	277	49	211
			(5.28)	(5.14)	(6.07)	(6.10)									(3.04)	(3.43)		
S4	4	0.7	2559	3460	217	418	57	172	19	106	6	45	0	2	82	325	62	248
			(5.05)	(5.12)	(6.10)	(6.14)									(3.34)	(3.47)		
S5	7	0.7	2311	3445	186	393	49	162	15	105	5	34	0	2	69	303	52	231
			(5.23)	(5.29)	(6.25)	(6.16)									(3.06)	(3.65)		
S6	10	0.7	2217	3424	180	386	44	146	12	82	3	27	0	1	59	256	45	195
			(5.13)	(5.27)	(6.24)	(6.37)									(3.54)	(3.37)		
S7	4	0.9	2541	3420	214	407	52	171	19	110	6	37	0	1	77	319	58	243
			(5.26)	(5.16)	(6.05)	(6.02)									(3.09)	(3.23)		
S8	7	0.9	2300	3410	181	386	48	157	15	84	4	27	0	1	67	269	51	205
			(5.12)	(5.23)	(6.13)	(6.24)									(3.42)	(3.17)		
S9	10	0.9	2172	3039	177	356	41	139	11	76	3	32	0	2	55	249	42	190
			(5.02)	(5.29)	(6.30)	(6.12)									(3.36)	(3.15)		

*From front roller nip, C indicates control sample (ring yarn spun without using nozzle), U- Upward airflow, D- Downward airflow.
Values in the parenthesis indicate CV%.

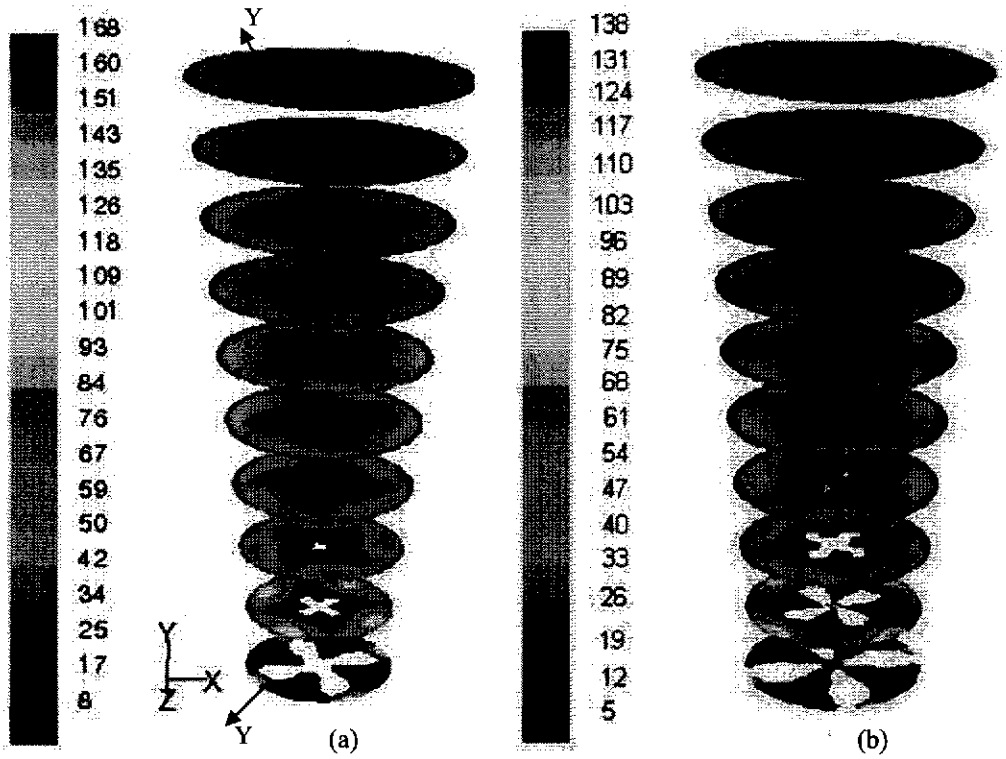

*White color shows velocity magnitudes of -1, & -2 m/s for (a) and (b)

Figure 9. Contours of tangential air velocity (m/s) of the nozzles: (a) 40°, 2.2 mm (b) 40°, 2.6 mm [Source: reference 22]

negative tangential velocity was observed (negative tangential velocity rotates the yarn in a clockwise direction). This negative tangential velocity may create ballooning in yarns similar to two nozzles in air-jet spinning, where the vortices were counter rotating [39]. Due to this ballooning action yarn positioning at the center of the nozzle would be difficult and hence wrapping of hairs and untwisting of the yarn would suffer [1, 22]. Some additional surface fibers may be generated by yarn rubbing due to the tendency of the yarn whirling towards the inner wall of the nozzle by the presence of the gradient of tangential air velocity (increasing tangential velocity from nozzle axis to inner wall of the nozzle). Due to the above action, some hairs on yarn surface may partly escape from the wrapping process. The nozzle having yarn channel diameter of 2.2 mm gave a larger reduction in hairiness, as the number of sections in the nozzle where ballooning action is created was three as compared to nozzle with channel diameter of 2.6 mm, where the numbers of such sections were four as shown in Figure 9 [22]. As the yarn spent somewhat longer duration in the ballooning region in the nozzle having yarn channel diameter of 2.6 mm this may reduce the efficiency of hairiness suppression. However, the magnitude of the negative tangential velocity was small (-1 m/s for 2.2 mm nozzle and -2 m/s for 2.6 mm nozzle) and hence its role was limited [22]. The intensity of swirling air was the predominant factor, rather than the small amount of negative air velocities on reduction in yarn hairiness [20].

The difference between the S3 hairiness values of yarns spun through nozzles having 1.8 mm and 2.2 mm yarn channel diameters was not significant [1, 22]. The above trend was observed for all the yarns. The reduction in yarn hairiness was more sensitive with respect to varying the axial angles of air inlets rather than the change in yarn channel diameter [1, 22].

Reduction in S3 hairiness values (longer hairs of 3 mm and above) obtained through the nozzle-ring spinning was higher for coarser yarns compared to that for finer cotton yarns [22]. This can be attributed to the fact that with the increase in yarn linear density, the numbers of fibers in the yarn cross-section increases, so more protruding ends are available for the air to act upon, and subsequently there was higher reduction in hairiness. From a statistical point of view, the more the hairs presented to the nozzle; the more was the reduction in yarn hairiness by the nozzle [22].

Optimization of Nozzle Parameters, Fiber Linear Density and Air Pressure on Hairiness of Polyester Spun Yarns in Nozzle-ring Spinning

Box and Behnken factorial design [40-41] was used for the optimization of nozzle parameters, fiber linear density and air pressure for polyester yarns during nozzle-ring spinning [25]. Polyester fibers of 38 mm length were used to spin 30 tex Z-twisted yarns. For each sample, 1000 meters of yarn was tested at a speed of 50 m/min. Using 1.0, 1.2 and 1.4 denier fibers separately, three yarns were spun, thus fiber fineness was a variable in these three yarns of same count. The spinning parameters were as follows: spindle speed 14000 rpm, traveller type and number EM1 UDR 2/0, twist per inch (tpi) 12.97. For nozzle-ring spinning, air pressures of 0.5, 0.7 and 0.9 bar were selected. The axial direction of airflow in the nozzles was kept opposite to the direction of yarn movement. The selected nozzle parameters were:

- Axial angles of air inlets of 40°, 45° and 50° with constant yarn channel diameter of 2.2 mm.
- Yarn channel diameters of 1.8, 2.2 and 2.6 mm with air inlets having a constant axial angle of 40°.

The influence of air pressure and axial angle of air inlets on S3 hairiness values is shown in Figure 10 [1, 25]. With the increase in air pressure from -1.0 levels to 1.0 level, S3 hairiness values decreases. With the increase in nozzle axial angle from -1.0 to 0 levels, S3 hairiness values decreases, but from 0 to 1.0 level, S3 hairiness value increases. From the above contours the best result was found for 0.0 level of axial angle (45°); other levels i.e. -1.0 and 1.0 levels show more or less similar S3 hairiness values. CFD modeling has been used to describe the results by comparing total velocity of the nozzle with axial angle of 45° with that for nozzle having axial angle of 50°. All the measurements were made at constant air pressure of 0.5 bar. For this purpose 30 tex yarn diameter was measured and post processing simulation was done in order to analyze the total velocity acting on the yarn surfaces.

Figure 11 [1, 25] shows resultant (or total) velocity of air acting on yarn surface and hair at various distances measured along the axis of the nozzle, taking the neck of the nozzle (x = 0 and y = 0) as the origin. Air velocity Vty and Vth (near inner wall of the nozzle) represents resultant air velocity acting on yarn surface and hair, respectively. Results are given for nozzles with axial angles of 45° and 50°. The figure indicated that air was coming from the bottom of the nozzle with constant resultant velocity, while near the neck, resultant air velocity suddenly increased. This sudden increase in resultant velocity was due to the

presence of four air inlets, the air stream from them mixed up with the air coming through the entry of yarn channel creating a swirling effect. After that, the resultant velocity decreased due to the presence of the divergent portion of the nozzle, where the air diffused very quickly. The resultant velocity trends for the yarn and hair were similar except that hair was subjected to a higher resultant air velocity due to reducing velocity gradient from nozzle inner wall to axis of the nozzle. The resultant velocity of air acting on the surface of the yarn and hair in the case of the nozzle with 45° axial angle was higher than that of the nozzle with 50° axial angle. The swirling intensity created by nozzle with 45° axial angle was stronger than that of the nozzle with 50° axial angle, resulting in a greater reduction in yarn hairiness by the former. The combined effect of air pressure and nozzle axial angle on S3 hairiness values indicate that 0.0 level of nozzle axial angle (45°) and 1.0 level of air pressure (0.9 bar) gives the optimum zone in terms of reducing the hairiness of yarns [1, 25].

The S3 hairiness values increases with the increase in fiber denier [1, 25]. This can be attributed to the fact that with the increase in fiber denier, bending and torsional rigidities of the fiber increases and it was difficult for air currents to fold/bend and wrap the hairs. Also, rigid fibers have a greater tendency to protrude from the yarn surface giving higher hairiness. Although the number of fibers in yarn cross-section using 1.0 denier fibers was greater in comparison to yarn spun from 1.2 denier fibers, the torsional rigidity of the fibers was the major influencing factor contributing yarn hairiness during spinning. With the increase in air pressure S3 hairiness values were decreased. At high air pressure, as the swirling intensity of air inside the nozzle increases, the improved wrapping of fibers around yarn body results in the decrease in yarn hairiness. The combined effect of fiber denier and air pressure on S3 hairiness values indicate that -0.5 level of fiber denier (1.1 denier) and 1.0 level of air pressure (0.9 bar) give the optimum zone in terms of reducing the hairiness of yarns [1, 25].

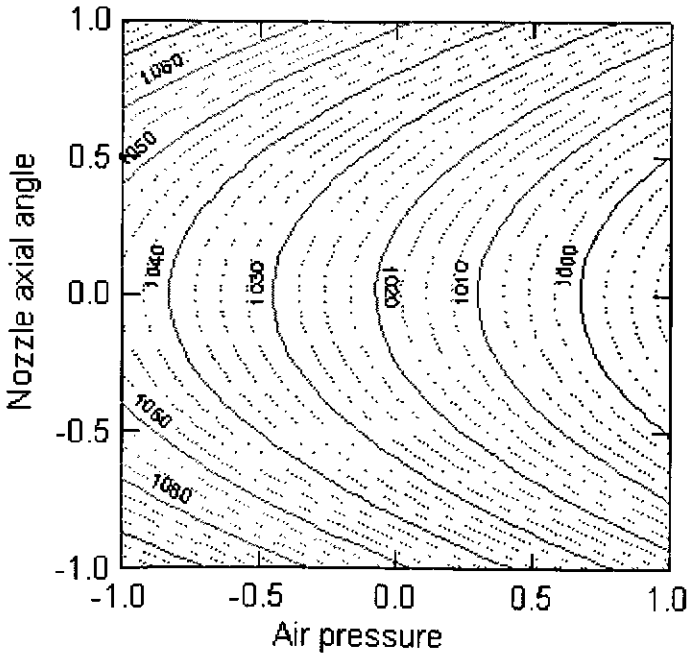

Figure 10. Influence of levels of air pressure and axial angle of air inlets on S3 hairiness values (per 1000 m) for yarn spun from 1.2 denier fibers [Source: reference 25]

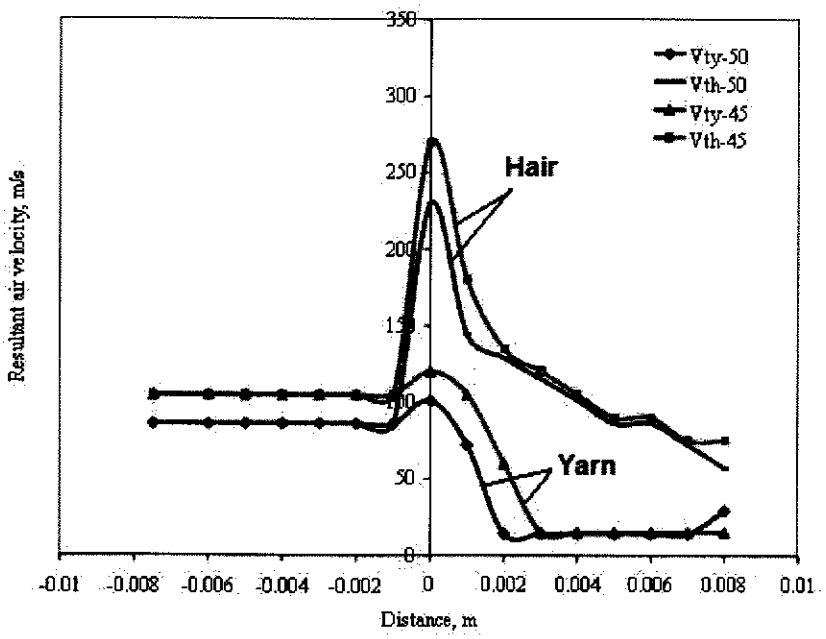

Figure 11. Resultant velocity of air acting on the surface of yarn and hair in the nozzles with axial angles of 45° and 50° [Source: reference 25]

Table 2. Hairiness values of ring and nozzle-ring spun yarns [Source: reference 22]

Sample codes (*Nozzle parameters)	Yarn Tex	Number of hairs/100 m length of yarn							% reduction in S3 hairiness values
		N1	N2	N3	N4	N6	N8	S3	
Ring yarn	10	2466	242	73	30	5	0	108 (3.10)	-
Ring yarn	20	2730	277	82	38	6	0	126 (3.23)	-
Ring yarn	30	2903	298	87	43	9	0	139 (3.29)	-
J1 (**40**, 2.2)	10	2269	205	41	16	3	0	60 (3.39)	44
J2 (**45**, 2.2)	10	2195	203	35	14	2	0	51 (3.14)	53
J3 (**50**, 2.2)	10	2318	213	44	17	3	0	64 (3.21)	41
J4 (**40**, 2.2)	20	2539	241	45	16	4	0	65 (3.05)	48
J5 (**45**, 2.2)	20	2457	232	44	11	3	0	58 (3.06)	54
J6 (**50**, 2.2)	20	2594	246	46	21	4	0	71 (3.17)	43
J7 (**40**, 2.2)	30	2642	253	43	17	5	0	65 (3.11)	53
J8 (**45**, 2.2)	30	2583	247	35	16	5	0	56 (3.05)	60
J9 (**50**, 2.2)	30	2729	259	45	20	6	0	71 (3.11)	49
J10 (40, **1.8**)	10	2274	208	42	17	3	0	62 (3.03)	42
J11 (40, **2.2**)	10	2273	206	41	16	3	0	60 (3.10)	44
J12 (40, **2.6**)	10	2275	207	44	18	4	0	66 (3.25)	39
J13 (40, **1.8**)	20	2539	241	47	17	4	0	68 (3.16)	46
J14 (40, **2.2**)	20	2542	240	46	17	4	0	67 (3.14)	47
J15 (40, **2.6**)	20	2548	243	49	19	5	0	73 (3.12)	42
J16 (40, **1.8**)	30	2643	257	43	17	5	0	65 (3.10)	53
J17 (40, **2.2**)	30	2639	255	42	17	5	0	64 (3.09)	54
J18 (40, **2.6**)	30	2646	256	45	19	6	0	70 (3.23)	49

*Axial angles of air inlets and yarn channel diameters. Values in the parenthesis indicate CV%.

Table 3. Angles of impact of air on hair of 1.1 mm length in nozzles [Source: reference 23]

Nozzle	0-plane				1-plane			
Type	R0	R0.33	R0.67	R1	R0	R0.33	R0.67	R1
Z40-2.2	0	0	10	17	0	6	28	30
Z50-2.2	0	5	23	35	0	5	20	40
Z60-2.2	3	9	40	52	8	8	35	48

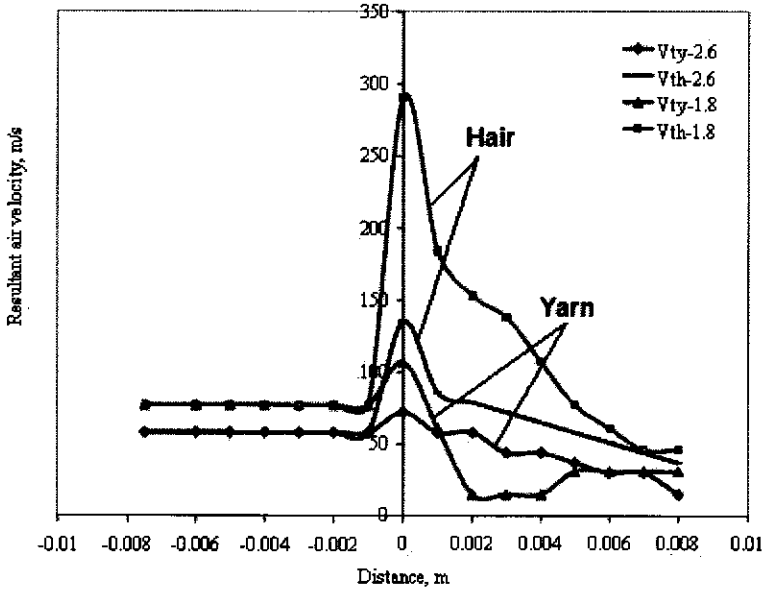

Figure 12. Resultant velocity of air acting on the surface of yarn and hair for the nozzles with yarn channel diameters of 1.8 mm and 2.6 mm [Source: reference 25]

With the increase in yarn channel diameter from -1.0 level to 1.0 level, yarn hairiness increases [1, 25]. Using CFD modeling, the nozzles with 1.8 and 2.6 mm yarn channel diameters were compared for resultant air velocity at an operating pressure of 0.5 bar. Air velocities Vty and Vth (near inner wall of the nozzle) represent resultant air velocity acting on yarn surface and hair, respectively as shown in Figure 12 [1, 25]. Higher air velocity was observed for both yarn and hair for nozzle with 1.8 mm diameter whereas the air velocity was much lower in the case of the nozzle with 2.6 mm diameter. The swirling intensity created by nozzle with 1.8 mm diameter was stronger than that of the nozzle with 2.6 mm diameter, which resulted in a greater reduction in hairiness by the former. The combined effect of nozzle diameter and air pressure on S3 hairiness values indicate that -1.0 level of nozzle diameter (1.8 mm) and 1.0 level of air pressure (0.9 bar) give the optimum zone in terms of reducing the hairiness of yarns. Nozzle axial angle plays more dominant role than the yarn channel diameter in reducing yarn hairiness [1, 25].

Effect of Air Drag and Angle of Impact on Reduction in Yarn Hairiness

The influence of air drag forces on reduction in yarn hairiness for a nozzle 40 at 0.5 bar is shown in Figure 13 [1, 23]. The longitudinal (LDH) and transverse (TDH) drag forces acting

on hair are shown. The x-axis notation 'distance' in Figure 13 means the length of the nozzle at the divergent section. For the hairs, the transverse drag forces were slightly higher than the longitudinal drag forces from planes 0 to 4 and a reverse trend was observed in planes 5 to 8. Bending and wrapping of hairs were most likely to take place at planes 0 to 1 due to the presence of high magnitude of forces. When the yarn leaves the divergent section and enters the cylindrical section of the nozzle, it re-twists itself due to false twisting and the hairs/fibers were wrapped in Z-direction. It shows the role of the drag forces in the reduction in yarn hairiness.

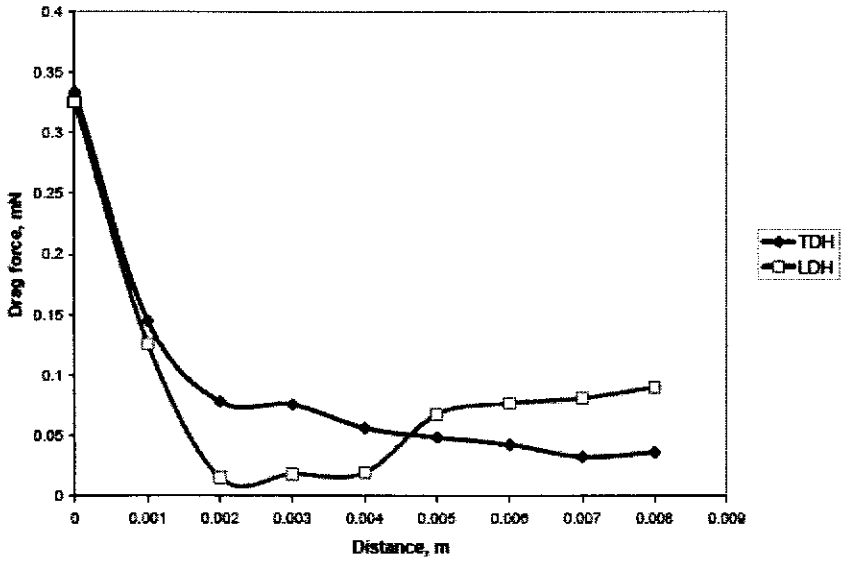

Figure 13. Longitudinal (LDH) and transverse (TDH) drag forces acting on hair [Source: reference 23]

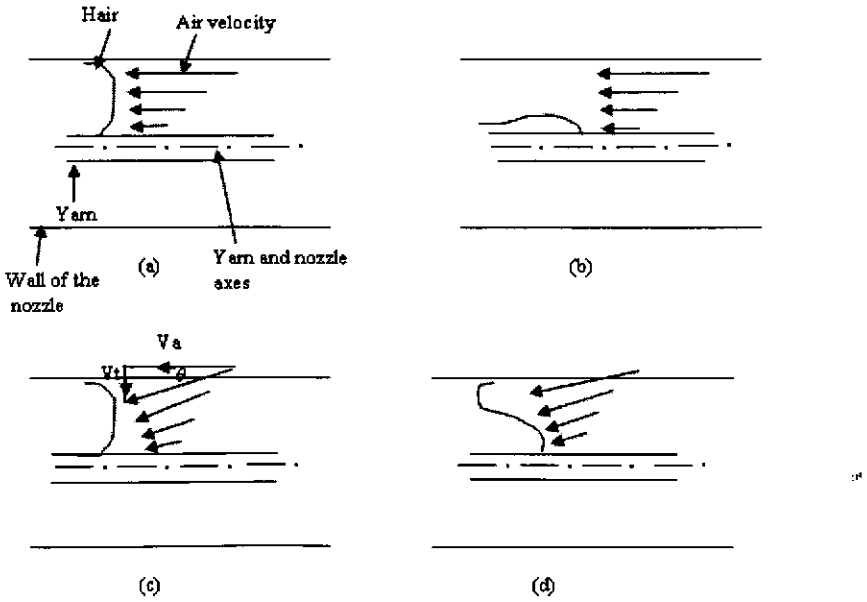

Figure 14. Schematic representation of curving of a protruding fiber/hair with respect to directions of air current: (a) & (b) zero angle of impinging; (c) & (d) high angle of impinging θ [Source: reference 23]

The influence of angle of impact (direction of impinging of air) on the hair for three nozzles Z40°, Z50° and Z60° was evaluated [1, 23]. These nozzles are suitable for Z-twisted yarns. 30 tex carded cotton yarns (Z-twisted) were produced with and without placing nozzle. Air pressures in the nozzles were kept at 0.5 bar. The directions of airflow in the nozzles were against the yarn direction during nozzle-ring spinning. The angle of air inlets decides the direction of impinging of air on the hair as well as on the yarn surface. The angle of impact is the tan^{-1} of the ratio of the tangential velocity to the axial velocity components of airflow. A hair with projecting length of 1.1 mm (from yarn surface to wall) was considered at 0-plane and this length was divided into four equal parts in the radial direction at R0, R0.33, R0.67 and R1, the R0 represents at yarn surface and R1 at inner wall of the nozzle. Tangential and axial velocities were obtained at these radial positions and impact angles were calculated [1, 23]. The values of the impact angle of air on hair at the 0- and 1- planes (where reduction in hairiness is most likely to take place) are shown in Table 3 [23]. The impact angle reduces from wall (R1) to centre (R0) at 0- and 1-planes for all the nozzles. Nozzle Z60 shows higher values of impact angle at the wall compared to other nozzles. When the impact angle was higher, curving of fibers occurred during the folding of hairs and the wrapping these curved fibers around the yarn surface would be difficult. A schematic representation showing curving of a protruding fiber/hair with respect to directions of impinging of air currents is illustrated in Figure 14. It has been reported that a larger axial angle of air inlets caused a longer air recirculation zone causing fiber curving (Figure 14c and Figure 14d), which might hinder the wrapping of hairs [29]. When the impact angle was less as in the case of nozzles Z40 and Z50, hairs might fold without much curving and wrapping around yarn becomes easier (Figure 14a and Figure 14b). This may be another reason (apart from air drag forces) for the higher reduction in hairiness as observed in the case of nozzle Z40 in comparison to Z50 and Z60 nozzles [23].

CONCLUSION

Air nozzles placed on a ring frame with upward airflow reduces hairiness of yarns in the range of 36-60% from the corresponding values of control yarns. From CFD analysis of airflow pattern and experiments a hypothesis on the mechanism of reduction in yarn hairiness was proposed. Airflow in downward direction increases the number of hairs in all the hair-length groups. A greater reduction in hairiness of yarns could be achieved with the use of higher air pressure; however, even at lower air pressure of 0.5 bar a considerable reduction in yarn hairiness was achievable. Placing the nozzle at 10 cm distance from the front roller nip was found to give improved yarn properties. The parameters obtained from simulation namely, velocity profile and trajectory gave important information for further analysis. Air velocities acting on yarn surface and hair were obtained. The swirling action in the nozzle was the reason for the reduction in yarn hairiness. The longitudinal and transverse air drag forces acting on the yarn surface and hairs also played a role in the reduction of yarn hairiness. Nozzle having a large axial angle of air inlets produced airflow with very high impact angle, leading to fiber curving during fiber folding and hence poor wrapping and consequently less reduction in yarn hairiness. Axial angles of air inlets played a major role in reducing the hairiness as compared to yarn channel diameters. Axial angle of air inlets of 45°

and yarn channel diameter of 2.2 mm (in the axial angle of air inlet series); axial angle of air inlets of 40° and yarn channel diameter of 2.2 mm (in the yarn channel diameter series) gave larger percentage reduction in S3 hairiness values for yarns. The percentage reduction in yarn hairiness by all the nozzles on coarser yarns was higher in comparison to the finer yarns. Increase in air pressure increased swirling intensity, thereby decreasing the yarn hairiness. Fiber linear density was a major influencing factor in reducing hairiness of polyester yarns during ring spinning. All the reductions in yarn hairiness were statistically significant. CFD modeling of airflow inside the nozzles gives a way forward in addressing the long outstanding problem on yarn hairiness.

Acknowledgement: The authors acknowledge Textile Research Journal, Indian Journal of Fibre and Textile Research, Journal of Textile the Institute, Fibers and Polymers, Journal of Textile and Apparel, Technology and Management, Indian Institute of Technology Delhi, Springer Science+Business Media, Taylor & Francis Group, http://www.informaworld.com and SAGE Publications Ltd for granting permission to reproduce some figures and tables used in this chapter.

REFERENCES

[1] Patnaik, A. Studies on Reduction of Yarn Hairiness Using Air Nozzles during Ring Spinning and Yarn Winding; PhD Thesis, *Indian Institute of Technology*, New Delhi, 2006, 1-208.
[2] Barella, A. *Text. Prog.* 1983, vol 13, 1-61.
[3] Barella, A; Manich, AM. *J. Text. Inst.*, 1988, vol 79, 189-197.
[4] Barella, A; Manich, AM. Text. Prog. 2002, vol 31, 1-44.
[5] Barella, A. In *Progress in Textiles: Science & Technology, Testing & Quality Management*; Kothari V. K; Ed; ISBN: 819010330X; IAFL Publication: New Delhi, 1999, Vol. 1, 232-303.
[6] Basu, A; Chellamani, KP. Ind. *J. Fiber. Text.* Res., 2000, vol 25, 163-168.
[7] Pillay, KPR. *Text. Res. J.*, 1964, vol 34, 783-791.
[8] Subramanian, TA; Grover, JM; Salhotra, KRJ. *Text. Inst.*, 1971, vol 62, 424-437.
[9] Tyagi, GK. Ind. *J. Fiber. Text.*, Res. 2004, vol 29, 35-38.
[10] Viswanathan, G; Munshi, VG; Ukidve, AV; Chandran, K. Text. *Res. J.*, 1989, vol 59, 707-711.
[11] Wang, X; Huang, W; Huang, XB. *J. Text. Inst.*, 1999, vol 90, 555-569.
[12] Ishtiaque, SM; Salhotra, KR; Kumar, AA. *sian Text. J.*, 2003, vol 12, 74-82.
[13] Kampen, W. Melliand Int. 2000, vol 6, 98-101.
[14] Artzt, P. Int. *Text. Bull.*, 1998, vol 44, 26-32.
[15] Ramachandralu, K; Subramanian, SN. Text. *Asia*, 2004, vol 35, 36-37.
[16] Rusch, A. *Melliand Int.*, 2000, vol 8, 247-248.
[17] Chellamani, KP; Arulmozhi, M; Vittopa, MK. *Asian Text. J.*, 2000, vol 9, 30-33.
[18] Stalder, H; Rusch, A. *Int. Text. Bull.* 2002, vol 48, 42-43.
[19] Cheng, KPS; Yu, C. *Text. Res. J.*, 2003, vol 73, 345-349.
[20] Patnaik, A; Rengasamy, RS; Kothari, VK; Punekar, H. *J. Text. Inst.*, 2006, vol 97, 97-101.

[21] Rengasamy, RS; Kothari, VK; Patnaik, A; Punekar, H. *J. Text. Inst.*, 2006, vol 97, 89-96.
[22] Patnaik, A; Rengasamy, RS; Kothari, VK; Ghosh, A; Punekar, H. *J. Text. App. Tech.* Mang., 2005, vol 4, 1-11.
[23] Rengasamy, RS; Patnaik, A; Anandjiwala, RD. *Text. Res. J.* 2008, vol 78, 412-420.
[24] Rengasamy, RS; Patnaik, A; Punekar, H. *Fibers Polym.*, 2006, vol 7, 317-322.
[25] Rengasamy, RS; Kothari, VK; Patnaik, A; Bhatia, SK. *Indian J. Fiber Text. Res.*, 2006, vol 31, 521-528.
[26] Patnaik, A; Rengasamy, RS; Kothari, VK; Ghosh, A; Punekar, H. Paper Presented in 4th AUTEX Conference, Roubaix, France, 22-24th June, 2004.
[27] Kalyanaraman, AR. *J. Text. Inst.*, 1992, vol 83, 407- 413.
[28] Wang, X; Miao, M; How, Y. *Text. Res. J.*, 1997, vol 67, 253-258.
[29] Zeng, YC; Yu. CW. *Text. Res. J.*, 2004, vol 74, 222-226.
[30] Cheng, KPS; Li, CHL. *Text. Res. J.*, 2002, vol 72, 1079-1087.
[31] Jeon, BS. *Text. Res. J.*, 2000, vol 70, 1019-1024.
[32] Patnaik, A; Rengasamy, RS; Kothari, VK; Bhatia, SK. *J. Text. Inst.*, 2008, vol 99, 17-27.
[33] Fluent 6.1, *User Guide;* 2003, Vol. 1, 1-31.12.
[34] Fluent 6.1, *User Guide*; 2003, Vol. 2, 1-31.12.
[35] Janna, W. Introduction to Fluid Mechanics; ISBN 10: 0534076327; *PWS Engineering:* Boston, MA, 1987; 2nd Edn, 1-680.
[36] Roberson, JA; Crowe, CT. *Engineering Fluid Mechanics*; ISBN 10: 0471147354; John Wiley & Sons: NY, 1996, 6th Edn, 1-689.
[37] Goldstein, S. *Modern Developments in Fluid Dynamics*; ISBN 10: 0486613585; Dover Publications Inc: Mineola, NY, 1998, Vol. 2, 1-702.
[38] Mack. C; Smart, JL. *J. Text. Inst.*, 1954, vol 45, T348-T362.
[39] Grosberg, P; Oxenham, W; Miao, M. *J. Text. Inst.* 1987, vol 78, 189-205.
[40] Box, GEP. *J. American Statistical Asso.*, 1959, vol 54, 622-654.
[41] Box, GEP; Behnken, DW. *Technomet.* 1960, vol 2, 455-475.